NANO LETTERS

2003
Vol. 3, No. 7
925−928

Epitaxial Directional Growth of Indium-Doped Tin Oxide Nanowire Arrays

Pho Nguyen,[‡] Hou T. Ng,*[,§] Jing Kong,[§] Alan M. Cassell,[§] Richard Quinn,[||] Jun Li,[§] Jie Han,[§] Melanie McNeil,[‡] and M. Meyyappan[†]

Center for Nanotechnology, NASA Ames Research Center, Moffett Field, California 94035, and Department of Chemical Engineering, San Jose State University, San Jose, California 95192

Received April 10, 2003; Revised Manuscript Received May 5, 2003

ABSTRACT

In this report, we show controlled in-situ doping of a single crystalline metal oxide nanowire, using indium-doped tin oxide (In–SnO_2) as an example, during a heteroepitaxial growth process. Highly regular and high-density arrays of In–SnO_2 nanowires, which demonstrate three- and four-fold growth symmetry, are obtained directly on optical sapphire substrates. Similar synthesis strategies, involving careful selection of desired growth conditions and smart manipulation of favorable thermodynamic properties, could be extended to production of various doped metal oxide nanowires.

Wide band gap metal oxide thin films such as ZnO, ZrO_2, SnO_2, In_2O_3, and CdO have an important role in numerous applications such as energy storage/conversion,[1] liquid crystal displays,[2] gas sensors,[3] and microelectronics.[4] In particular, the single crystalline nanowire form of these materials has been explored recently in nanoscale science and technology using various synthesis routes.[5] Although controlling the size of the nanowires can bring about changes in their optical and electronic properties, doping of the nanowires either through in-situ or postprocessing techniques will provide a far more favorable approach to modulate their properties. However, homogeneous introduction of dopants into the lattice matrices while preserving the structural integrity of the nanowires is a major challenge in metal oxide nanowire synthesis.

In the synthesis of the In−SnO_2 nanowires, a carbothermal reduction followed by a catalyst-mediated heteroepitaxial growth were used.[6] First, granular tin-doped indium oxide (10 wt % SnO_2 and 90 wt % In_2O_3, 99.99% purity) was mechanically pulverized and mixed thoroughly with graphite powder (99.99% purity) in a 1:1 weight ratio. The mixture was then placed upstream of a preannealed (1000 °C, 2 h) sapphire substrate inside a horizontal tube furnace. The substrate was coated with 2 nm thickness of gold (99.95% purity) via ion beam sputtering. Uniform nanowire growth was achieved at 840 °C with argon (Ar, 99.999%, 300 sccm) as the carrier gas.

Figure 1 shows scanning electron microscopy (SEM) images of arrays of In−SnO_2 nanowires on *a*-sapphire substrates. The nanowires exhibit wire-like geometrical shape with a relatively narrow diameter distribution (mean diameter = 86 nm ± 12 nm) and an average length of ∼ 2.5 μm. Most of the nanowires show a smooth surface morphology with well-defined facets and uniform diameter along the nanowire axis. Alloyed catalytic nanoparticles, either slightly larger or almost the same dimension as the nanowire diameter, are typically found at the terminating growth front, indicating their growth by the vapor−liquid−solid (VLS) mechanism.[7] Energy-dispersive X-ray spectroscopy (EDX) reveals these well-faceted nanoparticles to consist mainly of Au/Sn/In (∼ 71:6:23 atomic %).

The heteroepitaxial growth process allows intricate and complex cross-networks consisting of uniform In−SnO_2 nanowires on *m*-sapphire as well. Figure 1c shows a representative SEM image (top view) of a mesh-like nanowire formation. Higher resolution images further reveal formation of an almost regular matrix with nanowires growing mostly in directions orthogonal to each other. Interestingly, the network is a 3D structure consisting of individual nanowires as seen in Figure 1d; in contrast with previous SnO networks involving a different growth mode[8] which led to structurally connected junctions.

The nanowires are observed to project at ∼45 degrees with

* Corresponding Author. Telephone 650 604 6146; Fax 650 604 5244; E-mail: hng@mail.arc.nasa.gov.
[†] NASA Ames Research Center.
[‡] San Jose State University.
[§] Also at Eloret Corporation.
[||] Also at SETI Institute.

10.1021/nl0342186 CCC: $25.00
Published on Web 05/23/2003

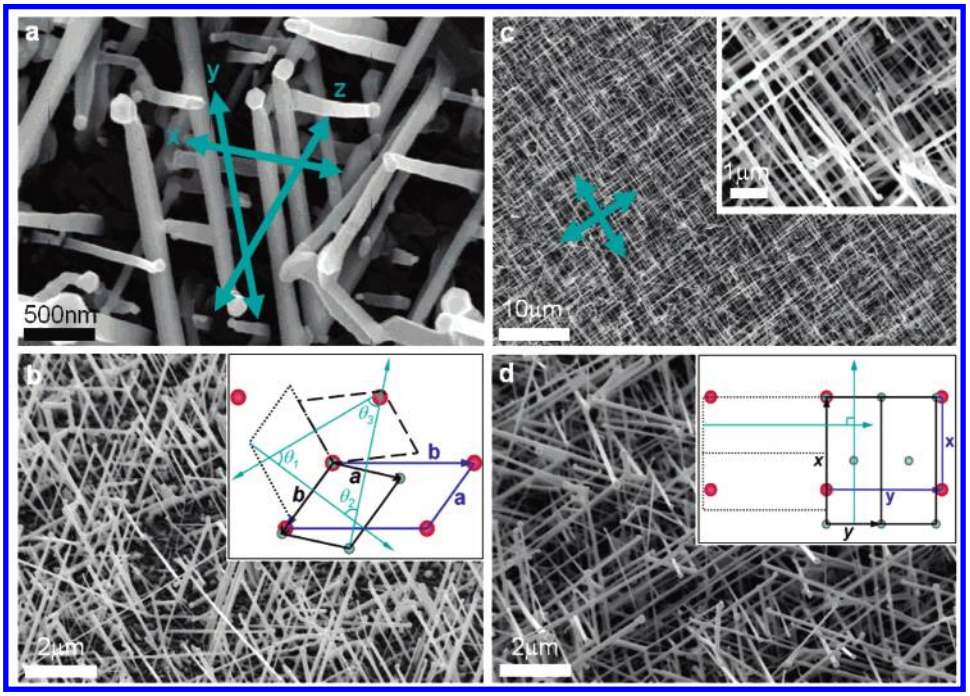

Figure 1. SEM images of In−SnO_2 nanowires on single crystalline optical sapphire substrates. (a) Top view of an array of nanowires. Nanosized catalysts at the ends of the nanowires can be clearly seen. The green arrows indicate main nanowire growth along *x*, *y*, and *z* directions. (b) Perspective view of the nanowires showing preferred directional growth on the same substrate plane. The inset shows an overlay of a unit cell of (110) plane (*a* face) of sapphire with that of (110) plane of rutile SnO_2. The atoms in solid red represent the oxygen atoms of sapphire while those in solid gray refer to the tin atoms of SnO_2. (c) Top view showing an intricate network of In−SnO_2 nanowires on a *m*-sapphire substrate. The inset shows a higher magnification of the network. (d) Perspective view of the nanowires shown in c. The inset is same as in b except with a unit cell of (100) plane (*m* face) of sapphire.

respect to the substrate plane, suggesting heteroepitaxial nanowire growth in preferred directions. Indeed, pseudo three- and four-fold symmetries, as indicated respectively by green arrows (Figure 1a and c), are observed. Since the In−SnO_2 nanowires possess a tetragonal rutile structure with preferred growth direction along the [100] direction (see Figure 3), minimum epitaxial lattice mismatch with (110) (*a* face) of optical sapphire could be achieved with its (110) plane as shown in Figure 1b. The unit cell of (110) SnO_2, represented by the gray Sn atoms with lattice constants *a* and *b*, is found to match reasonably well along three different directions (also the directions of (100) plane with respect to (110)) with that of the *a*-sapphire (lattice constants a and b) and found to agree with the experimental values. Lattice mismatches between *b*a, *c*a, and *a*a are calculated to be ∼6.03%, ∼6.03%, and ∼8.92%, respectively, with $\theta_1 = \theta_2$ (∼ 64.56°) and $\theta_3 \sim 50.88$. Indeed, these geometrical angles agree well with the experimental values. Due to mirror images of the unit cell, nanowires can be grown in opposite directions along each *x*, *y*, and *z* direction. We noticed that nanowire growth along the *x* direction is not as structurally uniform, most likely due to the larger lattice mismatch along this particular direction. On the (100) sapphire (*m* face), however, preferred lattice matches with SnO_2 (110) are found only along two major directions which are orthogonal to each other. Lattice mismatches between 2*y*y and *x*y are ∼ 1.89% and ∼ 3.14%, comparatively lower than on *a*-sapphire. This evidently explains the different directional growth phenomena and the more favorable growth leading to higher nanowire density in the latter. The angle between (110) and (100) of SnO_2 is calculated to be exactly 45°, which coincides well with the nanowires' projected angles.

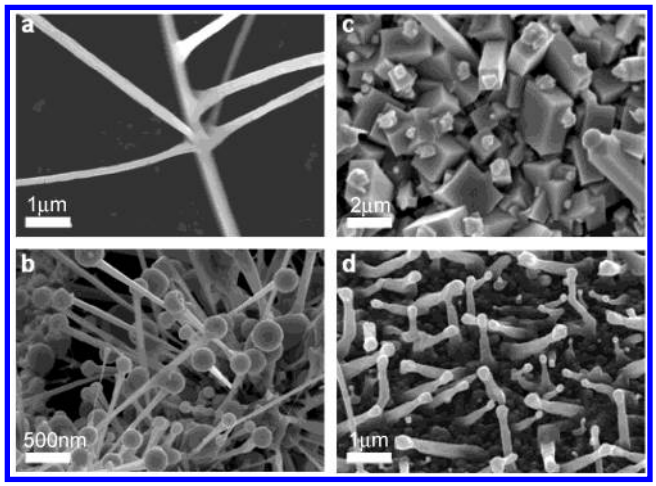

Figure 2. Scanning electron microscopy images showing examples of nanostructures that can be obtained by tweaking the experimental conditions. (a) A microsized structure consisting of nanowires forming a dendrimeric-like network (925 °C, 30 sccm, 1 h). (b) Nanostructures having microsized spheres with an extended shaft that resemble "nanopins" (875 °C, 300 sccm, 1 h). (c) An array of cubic submicrocrystals growing from a sapphire substrate (875 °C, 300 sccm, 2 h). Catalytic particles at the growth fronts can be observed. (d) Nanowires with irregular morphology grown on the substrate (870 °C, 30 sccm, 1 h).

There are a number of factors that can influence the morphologies of the synthesized products. For example, changes in the growth temperature, the flow rate of the carrier

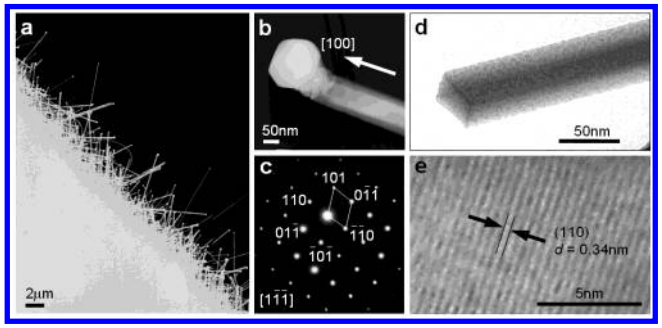

Figure 3. TEM images of the In−SnO_2 nanowires. (a) Low magnification image showing clearly the directional growth nature of the nanowires. (b) Image showing a single nanowire with a catalytic alloyed particle assuming a well-defined polygon. (c) SAED pattern of a nanowire. (d) TEM image showing a regular cross-section of a cleaved nanowire. (e) HRTEM image showing the lattice fringes corresponding to the (110) plane of tetragonal rutile SnO_2.

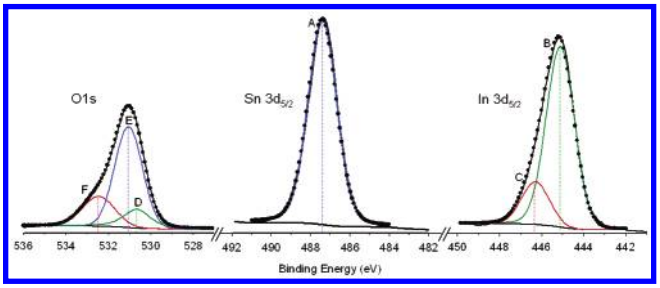

Figure 4. XPS spectra in the region of the Sn $3d_{5/2}$, In $3d_{5/2}$ and O 1s core levels of In−SnO_2 nanowires. The adventitious C peak at 285.0 eV was used to correct the binding energy positions of the peaks. A Shirley background correction was applied to each spectrum before the curve fitting. The extent of Gaussian−Lorentzian mixing was allowed to vary freely and the consistency in the curve fitting was maintained by executing the fits with different starting parameters. The peak sum of the fitted curves is represented by dotted circles.

gas, the reaction duration, and the nature of the substrate could yield products including cubic submicrocrystals, nanopins, and microsized dendrimeric nanowires (See Figure 2). Particularly, it is found that high quality single crystalline nanowires are predominantly obtained within a relatively narrow temperature range between 840 and 860 °C, an Ar gas flow rate between 250 and 350 sccm, and a feedstock source/substrate distance of separation of 1−3 cm.

TEM and HRTEM images provide further insight into the structure of In−SnO_2 nanowires. Figure 3a shows a TEM bright field image of a cross-section of an In−SnO_2/*a*-sapphire interface. The nanowires are projected at angles typically ∼45 degrees from the substrate plane and exhibit diameters between 50 and 80 nm, consistent with the earlier SEM images. Relatively long nanowires (> 10 μm) could be occasionally observed among the more uniform shorter nanowires. They are usually presented in the form of a single long nanowire. Enhanced growth at particular catalytic sites could have accounted for their formation. However, more in-depth studies are required to fully elucidate their growth phenomena. Alloyed nanoparticles are frequently found at the ends of the nanowires, as seen in Figure 3a and b, providing another evidence for the catalyst-assisted VLS growth mechanism. Although self-catalytic VLS nanowire growth via Sn catalytic particles formed through the so-called internal chemical reactions could possibly occur,[9] the absence of catalytic nanoparticles consisting solely of Sn from EDX analysis has ruled out such a possibility. The diameter of the nanowires is highly uniform and appears rather homogeneous and free of observable domain defects/boundaries, suggesting high single crystallinity of these nanowires.

A selected area electron diffraction (SAED) pattern (Figure 3c) of a nanowire taken perpendicular to its longitudinal axis further confirms the high single crystallinity. Regular diffraction spots could be indexed for the [1$\bar{1}$1] zone axis of single-crystalline tetragonal rutile SnO_2, with estimated lattice constants of $a = 4.685$ Å and $c = 3.200$ Å, which are close to those reported using powdered X-ray diffraction ($a = 4.737$ Å and $c = 3.186$ Å, JCPDS 88-0287). The incorporation of In atoms in the SnO_2 lattice structure does not seem to affect the highly uniform crystal packing. Physical deposition of In or In_2O_3 on the exterior of the nanowires is quite unlikely since well defined sharp side edges have been consistently observed under HRTEM. Similar electron diffraction patterns have been obtained over numerous In−SnO_2 nanowires and at different locations along the longitudinal axis of the nanowires. Figure 3d shows a rectangular cross-section of a nanowire whereby the alloyed tip is cleaved off, likely during the handling process. The well-defined crystal facets could be clearly seen, suggesting again the high crystallinity of the nanowires. A HRTEM lattice-resolved image of a representative nanowire further reveals that the nanowires are structurally uniform and single crystalline, with an interplanar spacing of 0.34 nm corresponding to the {110} plane of rutile crystalline SnO_2.

X-ray photoelectron spectroscopy further reveals the presence of In in the SnO_2 nanowires. The atomic concentrations of the chemical elements were calculated from the peak areas and indicated ∼5.7 atomic % of In, in close agreement with EDX analysis (∼6 atomic %). There are no significant impurities visible within the detection limit of the instrument and the adventitious C contamination is below 5 atomic %. Figure 4 shows a series of deconvoluted Sn ($3d_{5/2}$), In ($3d_{5/2}$), and O (1s) peaks of the In−SnO_2 nanowires. No distinct contributions due to metallic Sn and In are detected in respective spectra. The Sn ($3d_{5/2}$) peak is fitted with a single component A at 487.4 eV (fwhm = 1.7 eV) which corresponds to the Sn^{4+} ions in SnO_2. The peak corresponding to Sn^{2+} ion is not detected, which is typically downshifted from the Sn^{4+} peak by 0.7 eV.[10] In contrast, the In ($3d_{5/2}$) peak is deconvoluted into two major components. Peak B at 444.9 eV (fwhm = 1.59 eV) could be attributed to In_2O_3-like In while peak C at 446.2 eV (fwhm = 1.57 eV) to surface hydroxide and/or oxy-hydroxide species.[11] The latter is likely to arise from hydroxylation and/or incomplete hydrolysis of the surface oxide when the nanowires were exposed to ambient. As calculated from potentiometric electrochemical studies,[12] stability diagrams of the oxides have shown indium oxide to undergo hydrolysis more favorably than tin oxide at any pH, which explains the additional higher binding energy shoulder of the In ($3d_{5/2}$) peak.

The asymmetric O (1s) peak for the In−SnO_2 nanowires has been deconvoluted into three major components. Peak D at 530.6 eV (fwhm = 1.49 eV) is assigned to In_2O_3-like oxygen while peak E at 531.0 eV (fwhm = 1.54 eV) to SnO_2-like oxygen, which also constitutes the major component (highest intensity). Since the peak separation between $O-Sn^{4+}$ and $O-Sn^{2+}$ is marginal, formation of the distinct shoulder at the higher binding energy region is unlikely. Hence, the peak E at 532.5 eV (fwhm = 1.80 eV) is mostly likely due to presence of hydroxide, oxy-hydroxide- like oxygen, physiorbed water and oxygen atoms that were chemisorbed[13,14] on the surfaces of the nanowires.

The fact that SnO_2 is the major constituent of the synthesized nanowire despite the higher weight percentage of In_2O_3 in the feedstock deserves some discussion. In−SnO_2, nanowires are formed mainly through a two-step process, i.e., first, the formation of In and Sn vapor by competitive carbothermal reductions of respective oxides and, second, the growth of SnO_2 with in-situ doping of In following a VLS mechanism. Competitive carbothermal reductions of respective oxides are perceived to occur at the specific growth conditions according to

$$\frac{1}{x}M_xO_{y(s)} + \frac{y}{2x}C_{(s)} \overset{K_M}{\rightleftharpoons} M_{(g)} + \frac{y}{2x}CO_{2(g)}$$

where M = Sn or In and K_M is the equilibrium rate constant.

Based on the classical evaporation model of Hertz-Langmuir, and extended to the present dissociative evaporation process,[15,16] the flux of the metal vapor (which subsequently leads to the formation of metal oxides at the catalystic sites) can be expressed through the equivalent partial pressure, $P_{In(g)}$ or $P_{Sn(g)}$, corresponding to the hypothetical equilibrium of the reduction. Assuming an equimolar evaporation mode, the equilibrium constant can be expressed as:

$$K_M = P_M.P_{CO2}^{\,y/2x} = e^{(-\Delta G/RT)}$$

At T = 1113 K and after taking into consideration the initial ratio of SnO_2/In_2O_3 (10: 90 wt %), $P_{Sn}/P_{In} \cong 24$, which gives ∼5% atomic In, close to the measured dopant concentration of ∼5.7% in the In−SnO_2 nanowires. This unequivocally suggests that doping can be controlled by the thermodynamics of the competitive carbothermal reductions at a specific temperature and the initial ratio of In_2O_3 to SnO_2. We believe that doping or compositional changes in the synthesized nanowires can be controlled by preevaporation in a way similar to that in metallorganic chemical vapor deposition.

Hence, we expect building up of Sn vapor flux mainly with minor traces of In vapor at 840 °C. Subsequent transport by the Ar carrier gas to the reaction sites allows dissolution of Sn and In into the nanosized Au liquid droplets, which act as soft templates for directional nanowire growth. At the critical supersaturation point, SnO_2 nanowires begin to grow at the solid−liquid interface. Since control experiments with only In_2O_3/C at this particular condition yielded no noticeable nanowire growth, we believe that In atoms are likely to be introduced statistically at the Sn sites.

While using an individual ideal set of experimental parameters and maintaining a reasonably low vapor pressure, secondary nucleation events possibly leading to physical deposition of a mixture of oxides can be suppressed effectively. This approach has the potential to extend to other doped metal oxides to obtain low defect nanostructures, which are highly desirable for many practical applications that require good reproducibility, low defect density, controlled stoichiometry, and precise doping of the nanowires.

Acknowledgment. Work by ELORET and SETI authors was supported by NASA contracts. We are grateful to Dr. Ann Marshall of Stanford University for assistance in the TEM measurements.

References

(1) McBreen, J.; Srinivasan, S.; Khandkar, A. C.; Tilak, B. V. *Electrode Materials and Process for Energy Conversions and Storage*; Electrochemical Society: Pennington, NJ, 1997.
(2) Chigrinov, V. G. *Liquid Crystal Devices: Physics and Applications*; Artech House: London, 1999.
(3) Mandelis, A.; Christofides, C. *Physics, Chemistry and Technology of Solid State Gas Sensor Devices*; Wiley-Interscience: New York, 1993.
(4) Madon, M. J. *Fundamentals of Microfabrication: The Science of Miniaturization*; CRC Press: Boca Raton, 2002.
(5) Xia, Y.; Yang, P.; Sun, Y.; Wu, Y.; Mayers, B.; Gates, B.; Yin, Y.; Kim, F.; Yan, H. *Adv. Mater.* **2003**, *15*, 353−389.
(6) Ng, H. T.; Chen. B.; Han, J.; Meyyappan, M. *Appl. Phys. Lett.* **2003**, *82*, 2023−2025.
(7) Wagner, R. S.; Ellis, W. C. *Appl. Phys. Lett.* **1964**, *4*, 89.
(8) Wang, Z. L.; Pan, Z. *Adv. Mater.* **2002**, *14*, 1029−1032.
(9) Chen, Y.; et al. *Chem. Phys. Lett.* **2003**, *369*, 16−20.
(10) Szuber, J.; Czempik, G.; Larciprete, R.; Koziej, D.; Adamowicz, B. *Thin Solid Films* **2001**, *391*, 198−203.
(11) Donley, C.; Dunphy, D.; Paine, D.; Carter, C.; Nebesny, K.; Lee, P.; Alloway, D.; Armstrong, N. A. *Langmuir* **2002**, *18*, 450−457.
(12) Baes, C. F., Jr.; Mesmer, R. E. *The Hydrolysis of Cations*; John Wiley & Sons: New York, 1976; pp 319−327, 349−357.
(13) Mulla, I. S.; Rao, V. J.; Soni, H. S.; Badrinarayanan, S.; Sinha, A. P. B. *Surf. Coat. Technol.* **1987**, *31*, 77−88.
(14) Yea, B.; Sasaki, H.; Osaki, T.; Sughara, K.; Konishi, R. *Jpn. J. Appl. Phys.* **1999**, *38*, 2103−2107.
(15) Berman, A.; Epstein, M. *J. De Physique IV* **1999**, *9*, 319−324.
(16) L'vov, B. V. *Thermochim. Acta* **2000**, *360*, 109−120.

NL0342186